Construction and Building Materials 254 (2020) 119203

Contents lists available at ScienceDirect

Construction and Building Materials

journal homepage: www.elsevier.com/locate/conbuildmat

Rate dependent tensile behavior of polyurethane under varying strain rates

H.M.C.C. Somarathna [a,b,*], S.N. Raman [b,c,*], D. Mohotti [d], A.A. Mutalib [b], K.H. Badri [e]

[a] Department of Civil Engineering, Faculty of Engineering, University of Jaffna, Ariviyal Nagar, Killinochchi 44000, Sri Lanka
[b] Department of Civil Engineering, Faculty of Engineering and Built Environment, Universiti Kebangsaan Malaysia, 43600 UKM Bangi, Selangor, Malaysia
[c] Department of Architecture and Built Environment, Faculty of Engineering and Built Environment, Universiti Kebangsaan Malaysia, 43600 UKM Bangi, Selangor, Malaysia
[d] School of Engineering and Information Technology, The University of New South Wales, Canberra, ACT 2600, Australia
[e] School of Chemical Sciences and Food Technology, Universiti Kebangsaan Malaysia, 43600 UKM Bangi, Selangor, Malaysia

HIGHLIGHTS

- PU resins were prepared from the rapid reaction between PKO-p and MDI in the presence of PEG as the plasticizer.
- The uniaxial tensile characteristics under loading and unloading conditions and the cyclic softening behavior were examined.
- PUs are highly strain rate dependent and exhibits stress–strain non-linearity.
- The mechanical response of PUs can be described as hyper-viscoelastic.

ARTICLE INFO

Article history:
Received 19 November 2018
Received in revised form 11 April 2020
Accepted 13 April 2020

Keywords:
Dynamic loading
Polyurethane
Stress-strain behavior
Uniaxial tensile behavior
Varying strain rates

ABSTRACT

Elastomeric polymers, such as polyurethane (PU), are being used in novel applications to enhance the load-carrying capacity, ductility, and the survivability of structures under dynamic loading. The mechanical response of elastomeric materials is highly rate and pressure dependent, and exhibits stress-strain non-linearity. The objective of the current study is to identify the effect of the strain rate on the uniaxial tensile behavior of elastomeric PU. To this end, four types of PUs differing in their plasticizer content were used. The uniaxial tensile characteristics under loading and unloading conditions and the cyclic softening behavior were examined under varying strain rate regimes (ranging from 0.001 s^{-1} to 0.33 s^{-1}). The experimental results showed that the stress-strain behavior of all PUs is non-linear and rate dependent. Young's module, yield stress, tangent module, ultimate tensile stress, failure stress, failure strain, resilience module, toughness module and residual strain of PU6 at 0.33 s^{-1} are 0.37–4.13 times compared to the values at 0.001 s^{-1}. It also exhibits hysteresis and cyclic softening. Increasing strain rates resulted in a dramatic transition in behavior from rubbery to leathery for all PUs. This behavior was described as positive strain-rate dependence. The behavior of PUs was defined as hyper-viscoelastic material.

1. Introduction

Elastomeric polymers, such as polyurethane (PU) and polyurea, have extensive engineering applications in numerous industries, such as the building, vehicle, and infrastructure industries, the latter of which includes underground structures, marine construction. [1,2]. These materials are considered promising because of their high toughness-to-density ratio and their capability to resist large elastic deformations. Large strain recovery under a wide range of loading, including quasi-static to impact make these materials well suitable for the structures that are subject to varying loads [2–4]. In addition to their high structural capacity, energy absorption and dissipation capacity, these materials provide superior resistance against severe environmental conditions [1]. Recently, these elastomeric polymers were used in applications involving high strain rates, such as mechanical capacitors, the

Abbreviations: ASTM, American Society for Testing and Materials; HS, Hard Segments; MDI, 4,4-diphenylmethane diisocyanate; PEG, Polyethylene glycol; PKO-p, Palm-based polyol; PORCE, The Polymer Research Centre; PU, Polyurethane; SHPB, Split Hopkinson Pressure Bar; SHTB, Split Hopkinson Tension Bar; SS, Soft Segments; Ur, Resilience Modulus; Ut, Toughness Modulus; W, Work input.

* Corresponding authors at: Faculty of Engineering and Built Environment, Universiti Kebangsaan Malaysia, 43600 UKM Bangi, Selangor, Malaysia.
E-mail addresses: hmccsomarathna@gmail.com (H.M.C.C. Somarathna), snraman@gmail.com (S.N. Raman).

https://doi.org/10.1016/j.conbuildmat.2020.119203
0950-0618/

wet-skid resistance of tire treads, and acoustic damping [2,3,5–8]. Also, several studies have demonstrated the potential of these polymer coatings as retrofitting and strengthening material in several types of structural materials and systems, on masonry structures [9,10], metallic structures [11–15], composite structural systems [5,16,17], and reinforced concrete structures [18,19] to enhance the resistance of structures against impact or blast loadings. These elastomeric polymers dissipate energy via two major mechanisms, i.e., their viscoelastic behavior and the pressure- and strain-induced transition from the rubbery to glassy state, which makes them well-suited for the aforementioned applications [5,20]. In this study, a series of experimental investigations was undertaken to analyze the feasibility of bio-based PU elastomers, which were synthesized (solution casting process) as coatings for structural strengthening application in enhancing the resistance of reinforced concrete structures against impact or blast loading. The mechanical responses of brittle concrete shows relatively low failure strain under dynamic condition, hence strain energy is dominant [19,21]. The PU coating behaves as an additional membrane attached to concrete surface of the structural element when the load is applied. In addition, PU resin wet the concrete surface effectively and penetrate through the porous structure within the concrete due to its low viscosity, and allow contact with the uneven concrete surface. This in turn will enhance the toughness, strain capacities, and overall ductility of structural members such as slabs and beams. [3,19,21]. When ductile PU coating is applied onto the load-receiving face with respect to impact, load and pressure will have to pass through the PU layer before reaching the concrete element. A portion of the energy is absorbed and dissipated through its elastic plastic deformation before being transferred to the concrete element. The coating is applied on the compression side; hence, the stiffness of PU significantly increases compared with that under tension, thereby subsequently increasing the amount of absorbed energy. When PU coating is applied onto the rear-face, loads and pressure will have pass through the concrete element before reaching the PU coating; part of this energy is transferred to the PU, thereby compressing it, increasing stiffness of the concrete, and subsequently, increasing the amount of the absorbed energy. Then, the loads and pressure pass through the PU layer and are reflected on it free face as tensile release waves, thereby significantly decreasing the shear stiffness of the PU, and concurrently, substantially increasing its dissipative capability as a result of its viscoelasticity [3,14,19,21,22]. Thereby minimizing the incidents of debris flying away upon impact and resulting in casualties [3,19,21]. In addition, the use of elastomeric polymers provides better solutions than conventional and advanced techniques; hence, it is cost-effective (low capital cost and low resource consumption) and applicable to existing structures.

PU is a product of the rapid reaction of a monomer featuring at least two isocyanate functional groups with another monomer that contains at least two alcohol groups [2,3]. The resulting PU is a copolymer that contains alternate sequences of soft segments (SS) and hard segments (HS), and these domains are interconnected by main valence chains (Fig. 1) [23–28]. Generally, two types of dispersed HS morphologies are present: fibrillar domains (in which the domain axes are the same as the polymer chain axes) and lamellar domains (in which the domain axes are at right angles to the polymer chain axes) (Fig. 1). These HS domains link the linear polymer chains in both directions, forming a cross-linked network that governs the elastic properties [28]. In addition, these elastomers are cross-linked by secondary valence bonding within the domains, such as hydrogen bonding (with adjacent molecules via urethane –NH–CO–O– linkages), dipole interactions and van der Waals interactions [25]. Although the dissociation energy of secondary valence interactions is weaker than that of the main valence bond by one or two orders of magnitude, they increase

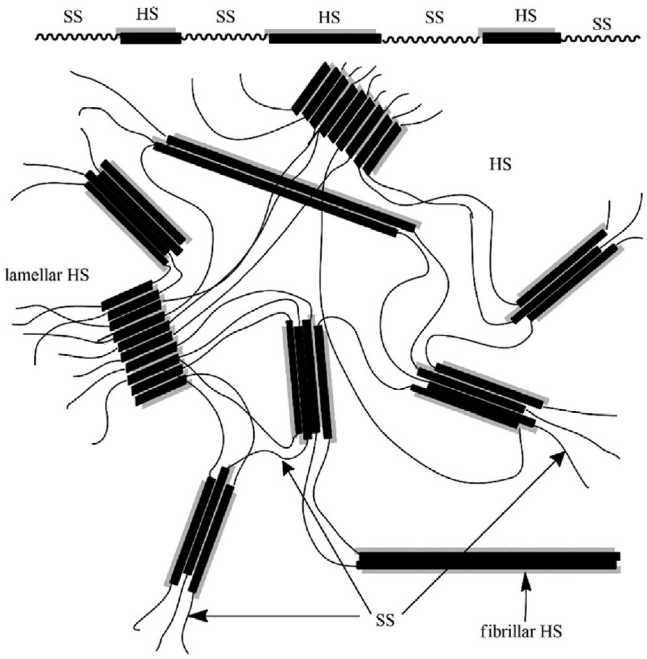

Fig. 1. Schematic scheme of segment arrangement in a polyurethane elastomer (HS, hard segment; SS, soft segment) [31].

crosslinking, control the segment mobility and provide high thermal and mechanical stability compared with the stability of conventional cross-links with only main valence bonding [25]. Thermodynamic incompatibility due to the low glass transition temperature (below ambient) of SS and the significantly higher glass transition temperature (above ambient) of HS caused by rigid aromatic molecules are responsible for phase separation in these domains. Specifically, the HS segments are in a glassy state, whereas the SS segments are in a rubbery state at ambient conditions. The dissimilar characteristics of these segments result in broad variations in their properties, and dramatic variations in properties can be obtained by altering the ratios of HS and SS in PU. In addition to chemical interactions, phase separation due to the physical arrangement of the molecules significantly affects the mechanical properties. To achieve required elastomeric performance in respective applications, the ratio of SS and HS must be tightly controlled [29]. However, the mechanical properties of PUs are not only influenced by the chemical interaction and molecular structure. The properties of PU elastomers also strongly depend on many other factors, including temperature, pressure, and the applied loading rate. Elastomeric polymers, which are subject to high strain rates above the ductile-to-brittle transition, may fail radially in a brittle manner under these conditions [30]. Hence, the non-linear, rate dependent and inelastic/plastic behavior constitute a major challenge in the selection of a suitable material for applications under varying loading conditions, and investigating the behavior of these materials over wide strain rates to simulate quasi-static and dynamic loading conditions is consequently of high importance.

The quasi-static behavior of PU elastomer has been characterized in several studies [23,24,40,32–39]. Although elastomers can be linearly viscoelastic at large strains, using Boltzmann superpositioning theory to deduce the properties at intermediate to high strains based on quasi-static values is not appropriate [41]. Furthermore, the mechanical performance of elastomers under essentially quasi-static conditions can be evaluated using several specifications and procedures, but standard test methods to evaluate their dynamic response are scarce because maintaining

homogeneous strain at higher strain rates is difficult. Various instruments have been utilized to evaluate the dynamic response of elastomeric materials, such as the universal test machine [42,43], the high speed impact or drop hammer testing system [44], the Hopkinson bar testing system [6,7,52,41,45–51], a special video-controlled tensile testing system [53], various servo-hydraulic testing systems [54,55], the screw drive mechanical tester, the Taylor impact tester [44,56] the Dynamic-Tensile-Extrusion tester [30] and other types of modified high speed test configurations [57,58]. Qi and Boyce [35] studied the uniaxial compression behavior of thermoplastic PU under varying strain rates (0.01, 0.05, 0.1 s^{-1}), and highly rate dependent stress–strain behavior was observed. Stress enhancement was observed as the strain rate increased, and the unloading curves were less dependent on the rate than the load curves. Yi et al. [45] studied the viscoelastic tensile behavior of three types of PUs using the split Hopkinson pressure bar (SHPB) system and stated that the PUs displayed a highly non-linear stress-strain relationship with significant hysteresis and rate dependency. Sarva et al. [46] systematically studied the compressive stress-strain behavior of a PU and a polyurea at strain rates ranging from 10^{-3} s^{-1} to 10^{4} s^{-1}. A Zwick screw drive mechanical tester was used for low to moderate (10^{-3}–10^{-1} s^{-1}) strain rates, an enhanced servo-hydraulic axial testing machine (MTS 810) was used for moderate to intermediate (1–10^{2} s^{-1}) strain rates, and two SHPB configurations were utilized for higher (10^{2}–10^{4} s^{-1}) strain rates during the compression testing. Recently, Fan et al. [6,7,59] investigated tensile characteristics at high strain rates (2700 s^{-1}), and the strain rate dependency (600–3800 s^{-1}) of a soft PU elastomeric polymer material using a split Hopkinson tension bar (SHTB) setup. Castro et al. (2005) studied the tensile behavior of PU resin, by undertaking tensile test up to failure and tests with loading-unloading-reloading cycles in order to quantify elastoplastic behavior of the material. Properties were investigated at different displacement rate of 0.5, and 5, mm/min and the findings indicated that the PU exhibit a ductile (highly non-linear) behavior and can be categorized as a stiff adhesive [60]. Liao et al. [55] investigated the viscoelasticity behavior of transparent PU under varying strain rates (1–10^{2} s^{-1}) and at temperatures of −40 °C to 40 °C using a servo-hydraulic high-speed tensile machine. The Digital Image Correlation technique was adopted to measure all strains and strain rates in both quasi-static and dynamic tests. The experimental results showed that tensile stress–strain curves and failure behaviors are significantly temperature and strain rate dependent [55].

Additionally, elastomeric materials display dissimilar mechanical characteristics in tension and compression under both quasi-static and dynamic loading conditions. However, several methods have been adopted to gain insight into the dynamic response of the tested structures and materials; most investigations focused on the compression behavior, whereas fewer studies examined tensile characteristics because the mechanisms available for studying the tensile response of these materials and structures are limited. Apparently, these studies do not provide insight into the rate dependency of the modulus, energy absorption behavior, and fracture mechanics of PUs at varying strain rate conditions, behavior under cyclic loading. These gaps have been addressed in this study where the uniaxial tensile behavior of four types of bio-based elastomeric PUs were investigated under varying strain rates (0.001–0.33 s^{-1}) using a hydraulic universal testing machine.

2. Experimental program

2.1. Materials

Palm-based polyol (PKO-p) [61,62] was supplied by the Polymer Research Centre (PORCE) of the Universiti Kebangsaan Malaysia. 4,4-diphenylmethane diisocyanate (MDI) was obtained from Cosmopolyurethane Sdn. Bhd., Malaysia. Acetone (industrial grade) and polyethylene glycol (PEG: Mw 200 Da) were purchased from Sigma Aldrich (M) Sdn. Bhd., Malaysia.

2.2. Preparations of the PU elastomers

Four types of PU resins were prepared from the rapid reaction between PKO-p and MDI in the presence of PEG as the plasticizer via a solution casting technique; acetone served as a solvent in the pre-polymerization technique. These PUs were labeled PU2, PU4, PU6 and PU8 (PU6 indicates the PU that contained 6% w/w of PEG with respect to PKO-p content). The composition each PU was changed to vary the soft segment content, which enhanced the toughness by altering the content of plasticizer over a narrow range [29]. Table 1 lists the composition of each PU in this paper. PU resins were prepared as pre-cast sheets with a thickness of approximately 3 mm. Clear yellowish and bubble-free PU sheets were obtained and conditioned at ambient temperature for further characterization. Average densities of PUs showed only a small deviation from one another (1071.5–1079.3), and the average density is 1075 kg/m^3 for all types of PUs.

2.3. Dynamic tensile test configuration and procedure

The four types of PUs were tested under constant strain uniaxial tension using an Instron model 5566 testing machine and displacement (engineering strain rate) controlled conditions at different strain rates (different crosshead speeds were used to attain different strain rates) [Fig. 2(b)]. For the tensile testing, dumbbell-shaped specimens (Die C) were cut from the cured pre-cast PU sheets as specified in ASTM D 412: Method-A [Fig. 2(a)]. Each specimen was cut in the same direction in the pre-cast sheet to avoid the influence of anisotropy or grain directionality resulting from the direction of flow during preparation and processing. Because elastomeric materials are extremely sensitive to clamping pressure, all specimens were automatically clamped to the grips and tested at ambient conditions with uniform strain rates of 0.001, 0.005, 0.001, 0.05, 0.1, and 0.33 s^{-1} (the maximum grip velocity of the machine was 500 mm/min, which corresponds to a strain rate of 0.33 s^{-1} for the test specimens used). The actuator displacement was controlled by a computer using the Blue Hill ver. 2.5 software. Testing was carried out with three different conditions: until sample rupture to investigate the full scale behavior until their failure, 0.3 maximum strain and unloading to investigate the loading unloading behavior, and 5 load-unload cycles with 0.3 maximum strain to investigate the cyclic softening behavior (only for PU6).

Several precautions were taken to ensure the accuracy of the results. During the specimen selection, specimens with longer gauge section were used where the length of the arc section is small compared to the gauge length. In addition, the width of the gauge was selected to be smaller (by 24%) than the end section, which resulted the actual deformation to occur in the gauge section. These provide low additional deformation outside the gauge

Table 1
Compositions of PUs samples.

Sample	Soft segments		Hard segment
	PKO-p (w/w)	PEG (w/w)	MDI (w/w)
PU2	100	2	80
PU4	100	4	80
PU6	100	6	80
PU8	100	8	80

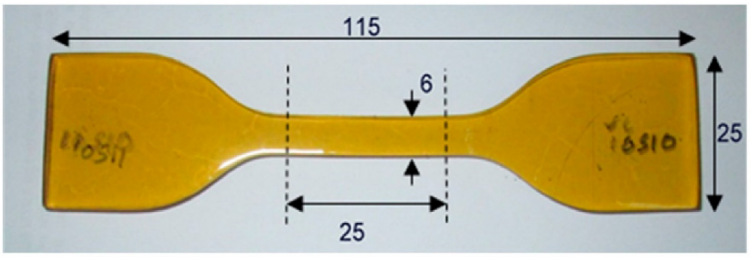

(a)

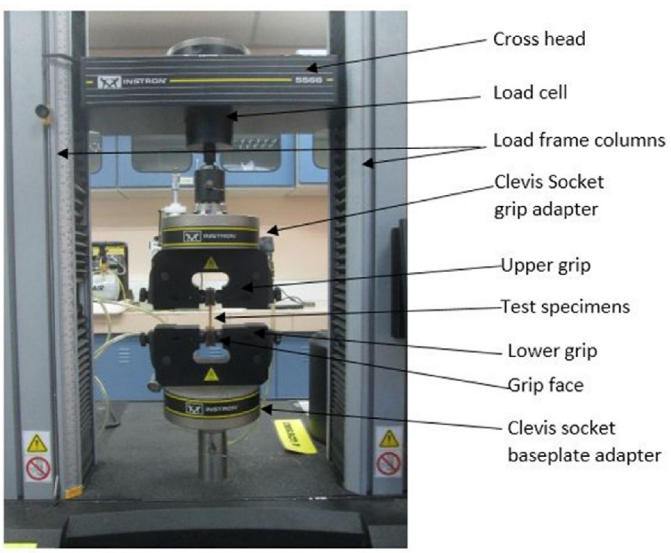

(b)

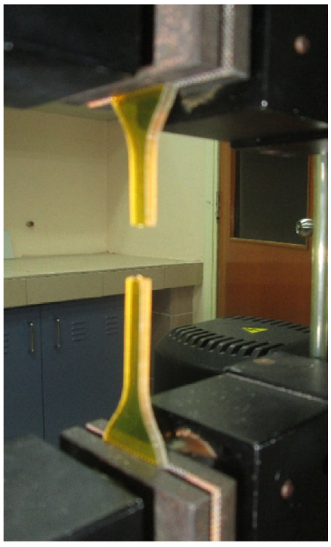

(c)

Fig. 2. The: (a) Tensile test specimens (Dimensions of specimens in mm); (b) Uniaxial tensile test setup; and (c) Tested specimen.

section and improve precision of the elongation measurement. The gauge length was marked in each specimen prior to the test and the failure location was checked after the test (Fig. 2(c)). Two other lines were drawn where the specimen was gripped, and those lines were checked after the test to ensure no considerable slippage at the grips of the test machine. Only the specimens which satisfied these conditions were selected for further analysis to investigate the properties. For each cases, a minimum ten samples were tested. The authors acknowledge that even after using careful measuring technique, this method can induce some minor inaccuracies in strain measurements, and duly acknowledge this limitation.

2.4. Data collection

The testing system acquired data (time, load, and deflection) using Blue Hill v2.5. Strain histories were obtained by converting the recorded displacement time histories. Correspondingly, stress histories were obtained based on the force time histories. The stress–strain relationships of each specimen were obtained from their individual time histories, and several uniaxial tensile properties of interest were computed from the obtained stress-strain data

3. Experimental results and discussion

In the following sections, the experimental findings are detailed and discussed. The locations of necking and failure were observed during the testing to ensure that they were within the gauge region, and only samples in which these failures occurred within the gage region were used for further analysis.

3.1. Tensile characteristics

The engineering stress and strain were calculated using the initial cross-sectional area, and the engineering stress-strain relationships were subsequently used to generate the true stress-strain plots. The true stress (Eq. (1)) and true strain (Eq. (2)) were calculated based on the instantaneous cross-sectional area, where true strain is the natural logarithm of the ratio of instantaneous length to initial length, and the instantaneous cross-sectional area was calculated by assuming PUs are bulk and nearly incompressible.

$$\sigma_T = \sigma_E(1 + \varepsilon_E) \tag{1}$$

$$\varepsilon_T = \ln(1 + \varepsilon_E) \tag{2}$$

where σ_E and ε_E are the engineering stress and engineering strain, respectively, and σ_T and ε_T are the true (Cauchy) stress and true (Hencky) strain, respectively.

The plots of strain rate vs. strain of PU6 for varying strain rates are shown in Fig. 3, and these plots are representative of those of the other PUs. The technical strain rate remained almost constant throughout the test for strain rates from 0.001 s^{-1} to 0.1 s^{-1} (see Fig. 3(a)). The initial region of the curve for a strain rate of 0.33 s^{-1} shows a small deviation at the beginning of the test because the specimens required $\approx$ 0.04 s to reach dynamic equilibrium, which corresponds to a strain of 0.33 s^{-1} for all PUs. Therefore the initial stiffness region of these curves of 0.33 s^{-1} strain

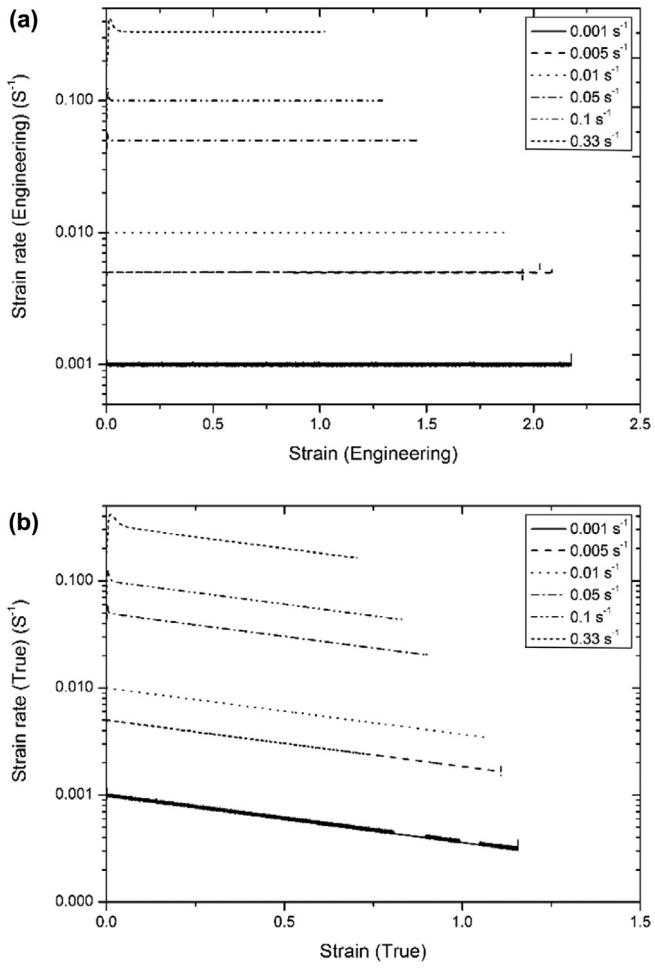

Fig. 3. The strain rate-strain curves of PU6 at varying strain rates; (a) Engineering, (b) True.

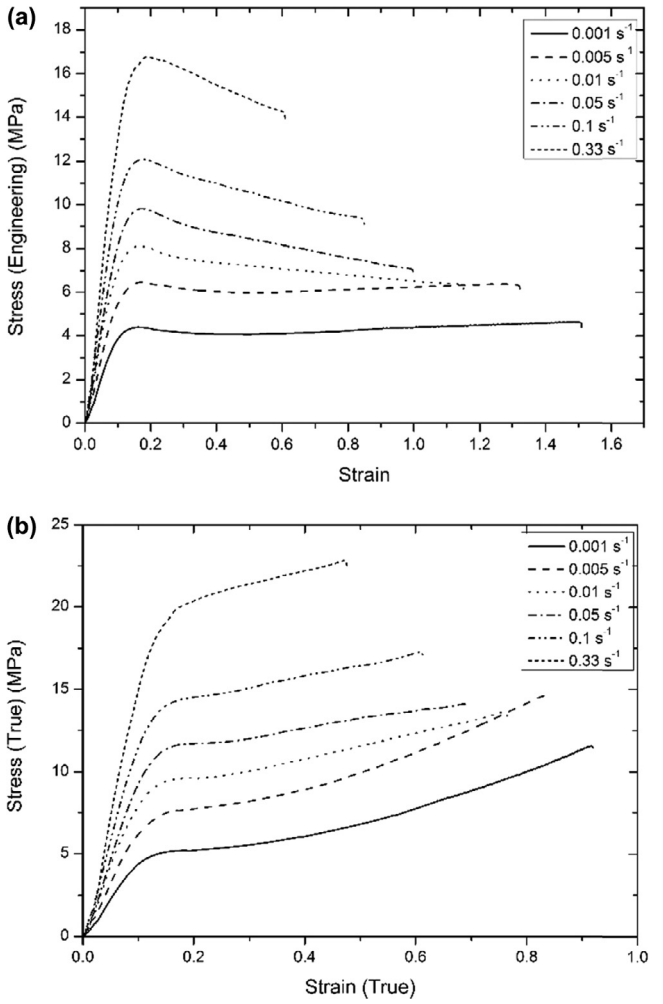

Fig. 4. The stress-strain curves of PU2 at varying strain rates; (a) Engineering, (b) True.

level, may not provide accurate data for nearly up to 0.04 s. However, all strain level tested produced a gradual decrease in the true strain rate due to the reduction in the actual cross sectional area over time (Fig. 3(b)). Non-linear stress–strain behavior was observed for all PUs, and the tensile responses (engineering and true stress–strain relationship) of PU2, PU4, PU6 and PU8 are shown in Figs. 4–7, respectively, for varying strain rates (0.001–0.33 s^{-1}). All PUs exhibited the behavior of a typical viscoelastic material in both their engineering and true stress-strain responses. The stress–strain behavior under varying strain rates displayed strong hysteresis behavior during loading for all PUs. This behavior is further supported by the outcomes shown in Figs. 8–12, which plot Young's modulus, yield stress, tangent modulus, ultimate tensile stress, and the stress and strain at failure as a function of the strain rate. Figs. 13–16 plot the tensile strain energy responses and their characteristics, explicitly, the cumulative strain energy density, the modulus of resilience and the modulus of toughness and their ratios at varying strain rates. In each case, representative tensile characteristics were evaluated using the experimental data, and the average value was calculated by taking the mean of five sets of tests based on the engineering stress-strain relationship.

During uniaxial tension, the SS domains of elastomeric PU facilitate the stress transfer to the adjacent HS domains [28]. Both the engineering and true stress-strain curves show a linear elastic region in the initial response for each case. The initial modulus significantly depended on the rate, and the results demonstrate a dramatic transition in the stiffness over the strain rate regimes tested: leathery behavior increased, and rubbery behavior persisted at high strain rates. This fact is consistent with the well-known effect of the strain rate on elastomers, i.e., the stiffness of an elastomer directly correlates with the strain rate. Several other researchers have observed similar phenomena [32,41,42,45–47,54]. Young's modulus is known to be governed by the strain rate, as illustrated in all PUs shown in Fig. 8 and Table 2, and this parameter significantly increased as the strain rate increased over the tested range for all four PUs. This phenomenon may have arisen because the time for re-aligning the molecular orientation towards a uniaxial direction was insufficient, which resulted in a dramatic stiffening effect. PU2, which featured the highest hard segment content (lowest plasticizer content), exhibited the highest initial stiffness (Young's modulus) for all strain regimes, and this value inversely correlated with the plasticizer (SS) content. Generally, the SS segments deform, whereas HS segments tend to resist changes in shape [63]. Additionally, the HS domains behave as crosslinking volumes with high functionality while simultaneously acting as a filler [25]. In general, crosslinking stability depends more on the stability of the HS domains and less on the contribution of the SS domain [25]. For high contents of HS, such as in PU2, the degree of crosslinking in the HS phase will be increased. Therefore, this high content of HS better retains its original shape, which consequently increases the stiffness during the deformation [63]. By extrapolating this nearly linear relationship to high strain rate conditions, such as strain rates exceeding 10 s^{-1}, it is possible to

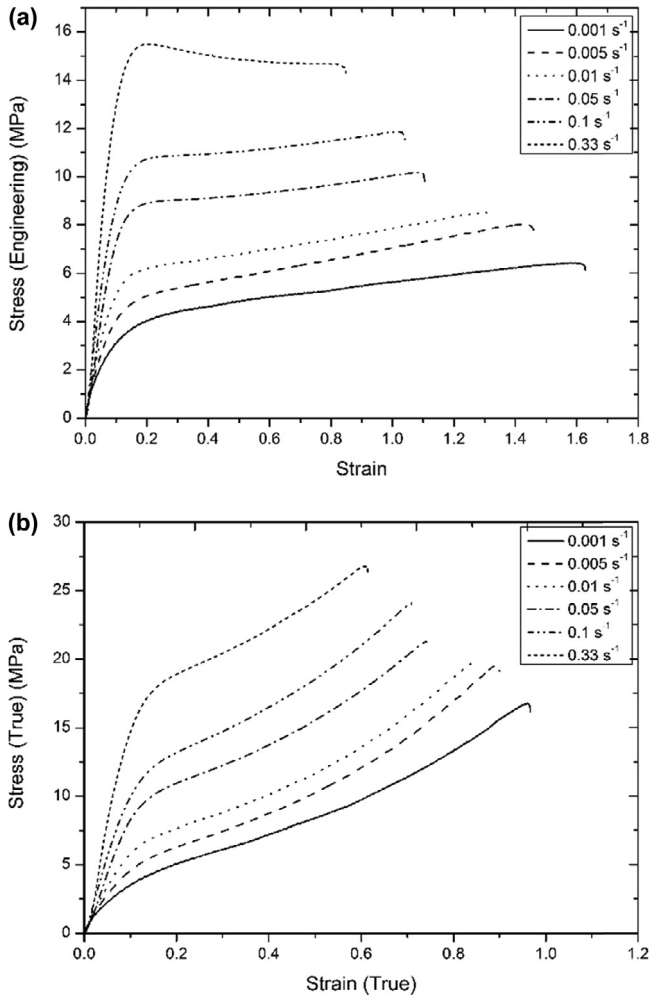

Fig. 5. The stress-strain curves of PU4 at varying strain rates; (a) Engineering, (b) True.

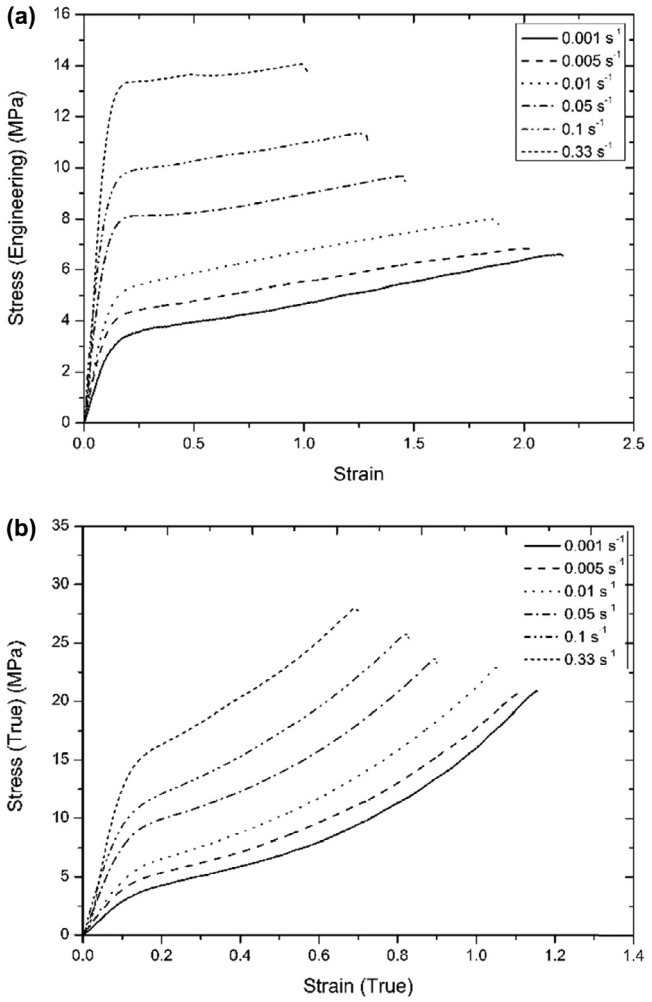

Fig. 6. The stress-strain curves of PU6 at varying strain rates; (a) Engineering, (b) True.

estimate Young's modulus for these PUs to show that high strains further increase this parameter.

After the linear stress–strain region, which showed substantial stress and elongation, the PUs began to yield, as shown in Figs. 4–7 for all strain conditions. In the stress-strain relationship which were obtained, a clear yield point is not apparent Therefore, proof stress at 0.5% strain has been obtained instead of yield stress (this is an approach that is similar to that adopted for most other ductile materials that do not show a proper yield point) [64]. Fig. 9 plots the relationship between the yield stresses over the tested strain rate regimes for low to intermediate strain rates. Over the tested range, the yield stress significantly increased almost linearly as a function of the logarithm of the strain rate for increasing strain rates (Table 3). However, the yield strains are nearly comparable over this range of strain rates. Specifically, the yield stress also showed variations similar to that of Young's modulus. PU2 exhibited the highest yield stress for all strain levels because it was stiffer than the other materials due to its high HS content.

The two types of HS domain morphologies (fibrillar and lamellar) differently influence the deformation mechanism of these materials. The long SS in the polymer chains are random coils, and the resultant matrix can be defined as a continuum. Initially, the HS domains will be orientated due to the stress transformation, and they tend to align their long axes in the stretching direction by rotating [25,28]. The deformation pathways of the HS domains depend on their physical properties and morphology. For the fibrillar morphology, the domains easily orient along the direction of chain extension because the long axis of the domain is same as the chain direction. In the lamellar morphology, the HS domain begins to rotate in order to align in the stretching direction because the long axis of the HS domain is perpendicular to the chain axis. The rotation of the lamellae in the HS domain dominates during the initial stage of deformation due to the low stresses, and the lamellar HS domain may break into smaller fragments or be destroyed due to stress transfer at higher strain conditions [28].

Generally, a change in the two-phase structure began at strains beyond yield point due to the breakdown of crosslinks and the fragmentation of the original hard domains into several smaller units, which resulted in permanent deformation of the material [63]. Bonart [25] suggested that the plastic deformation is caused by the sliding of HS domains relative to their adjacent domains within the hard domains (molecular chain scission or disentanglement) and the reduction of crosslinks per unit volume. Enderle et al. [26] attributed the phenomenon to two possible causes: the sliding of segments, which may result in irreversible deformation and consequent residual strain, and sliding, which may result in the stripping of segments from the hard domains and form a new soft matrix within the hard domains. All tested PUs displayed a brief period of yielding that resulted in inelastic deformation over all tested strain rates. Specifically, the tangent modulus signified the behavior of materials at stresses beyond their offset yield point.

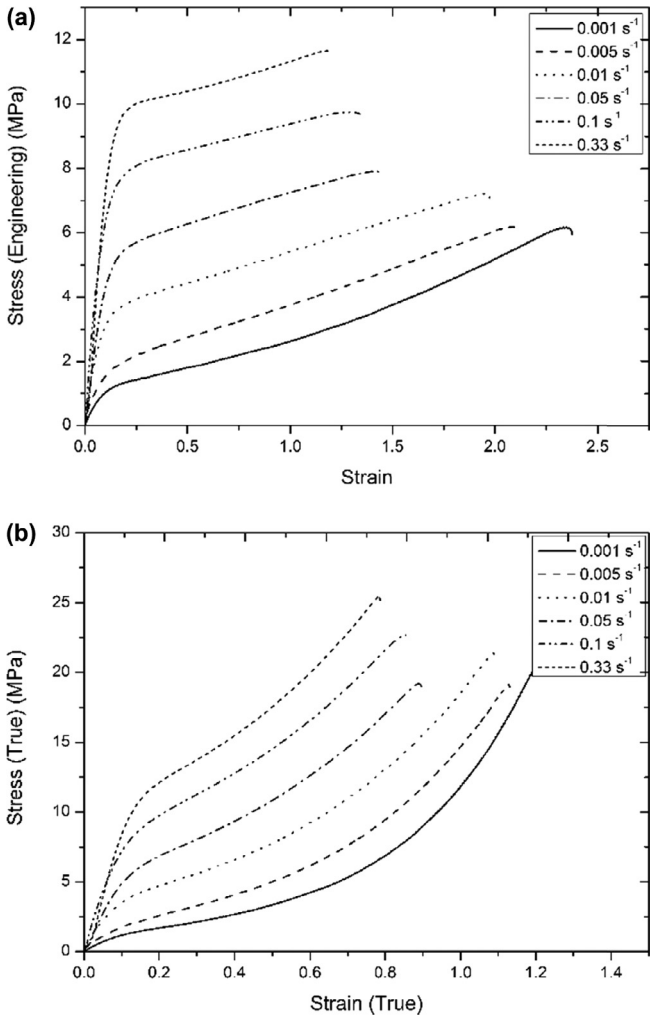

Fig. 7. The stress-strain curves of PU8 at varying strain rates; (a) Engineering, (b) True.

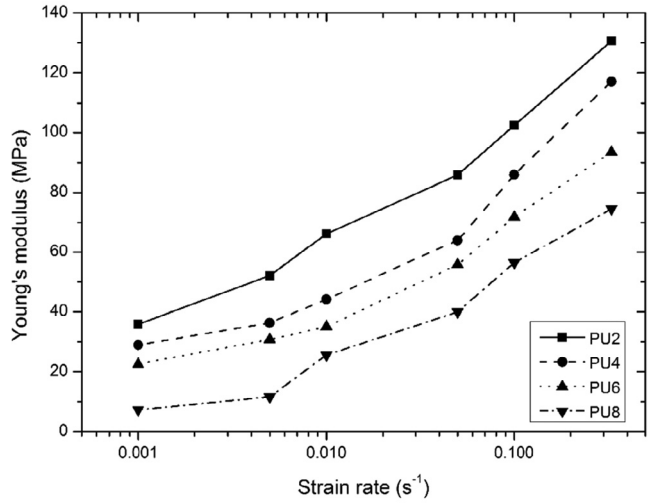

Fig. 8. The Young's modulus at varying strain rates.

Fig. 10 and Table 4 show the tangent modulus of PUs for varying strain conditions obtained in this study. For all PUs, the strain rate influenced the tangent modulus, and this relationship was gener-

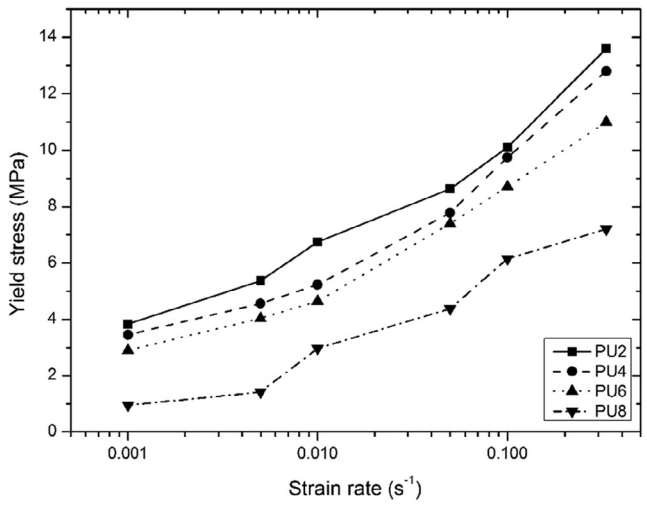

Fig. 9. The yield stress at varying strain rates.

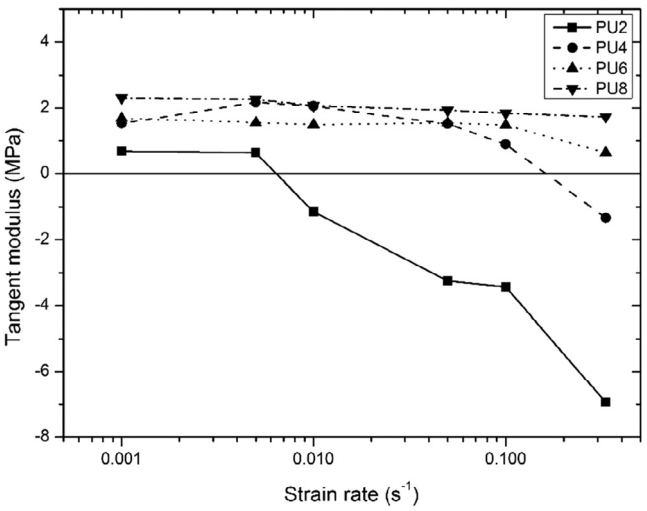

Fig. 10. The tangent modulus at varying strain rates.

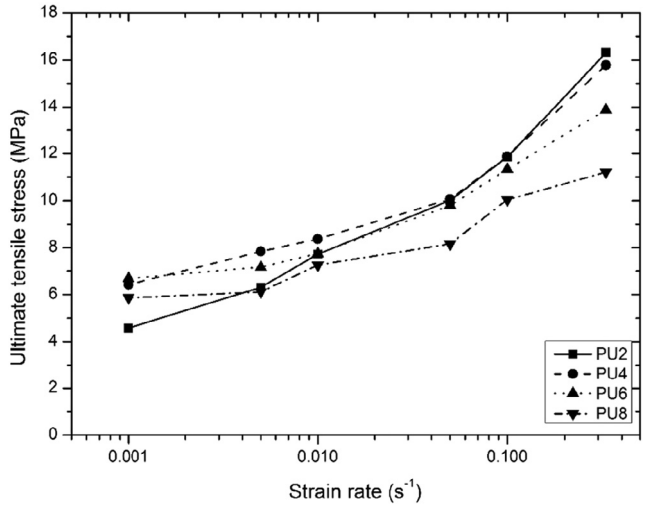

Fig. 11. Ultimate tensile stress at varying strain rates.

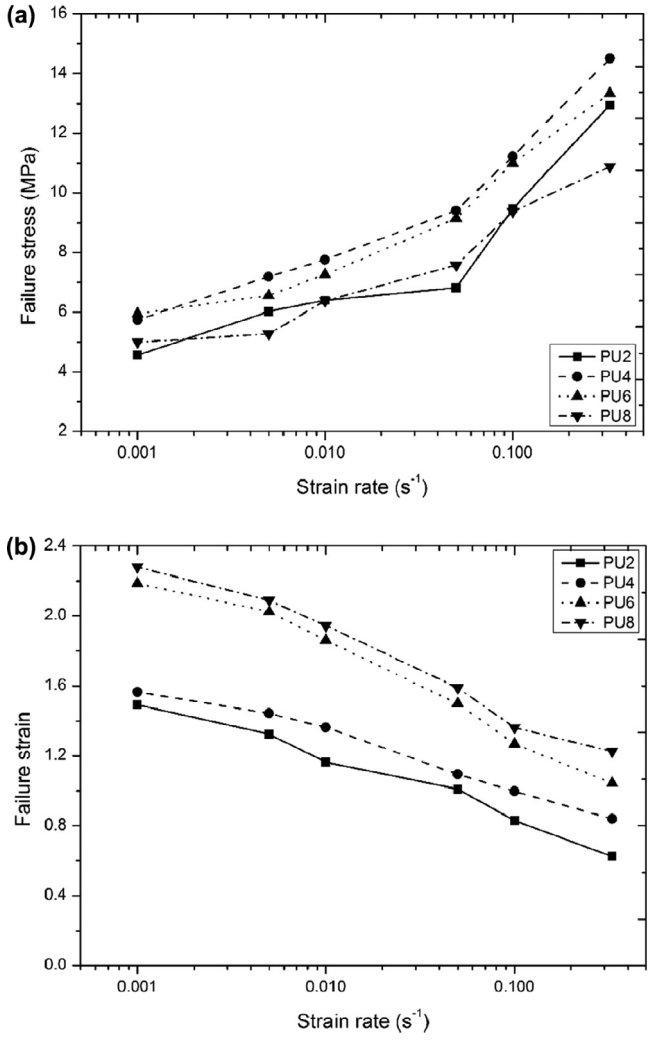

Fig. 12. (a) Failure stress, (b) Failure strain of PUs at varying strain rates.

ally inverse. PU2, which contained the lowest level of plasticizer (SS), showed a rapid reduction in the tangent modulus over the tested strain rates compared with other PUs. PU2 showed a negative value for strain rates higher than the 0.01 s^{-1}, and PU4 displayed a negative value for the 0.33 s^{-1} condition only. In other words, PU2 and PU4 have undergone strain softening behavior under these strain conditions. PU6 and PU8 displayed strain hardening for all strain rates tested in this study. Ductility increased from PU2 to PU8 due to the increase in the soft segment content. This trend was consistent with the change from strain hardening behavior to strain softening when the strain rate increased, which is caused by a decrease in the alignment of PU chains along the direction of elongation and by a loss of elasticity. Consequently, significant degradation and a reduction in crosslinks per unit volume were observed, which reduced the strain hardening behavior due to the rapid change in molecular structure when strain rate is increased. According to this relationship, the tangent moduli of these PUs likely further decreased at high strain rates, and PU6 and PU8 may have shown strain softening behavior at high strain rates. Specifically, all PUs yielded over a wide range of strains. Although all PUs underwent permanent deformation, they remained capable of withstanding further loads before their ultimate failure.

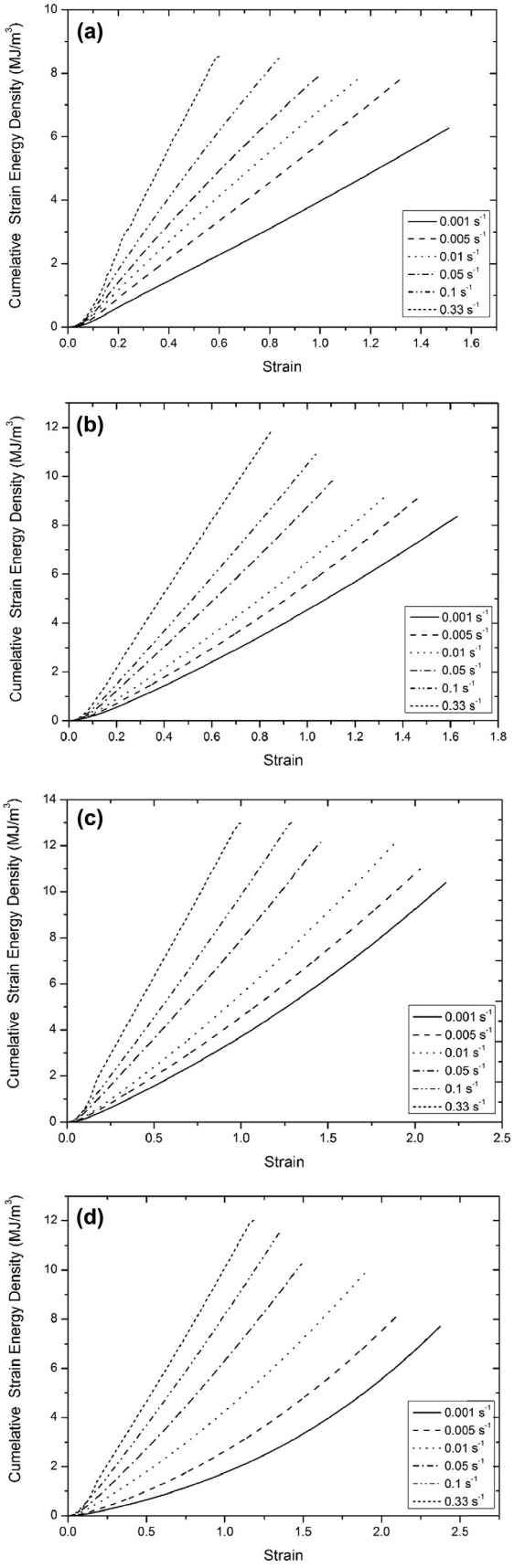

Fig. 13. Cumulative strain energy density vs. strain curves of PUs at varying strain rates; (a) PU2, (b) PU4, (c) PU6, (d) PU8.

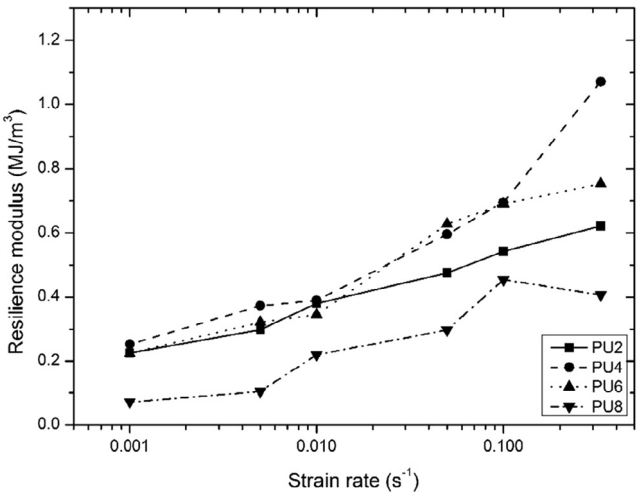

Fig. 14. The resilience modulus of PUs at varying strain rates.

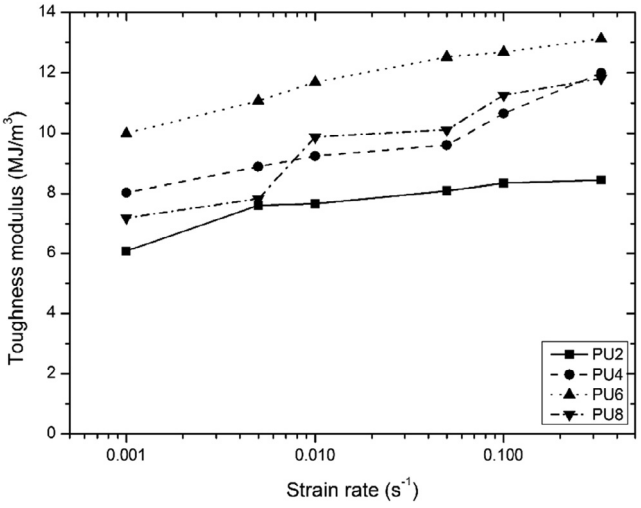

Fig. 15. The toughness modulus of PUs at varying strain rates.

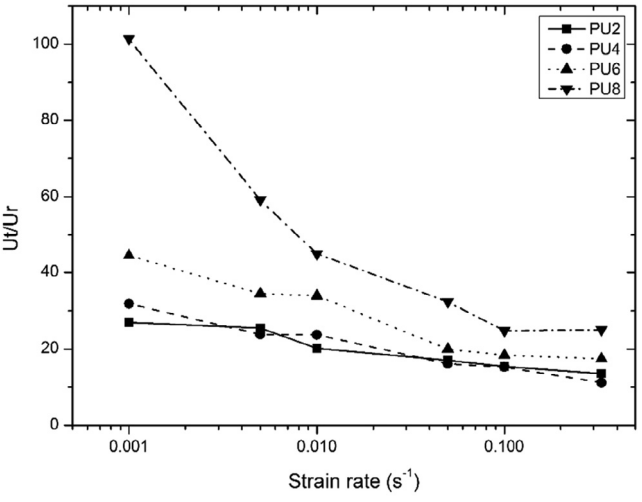

Fig. 16. The Ut/Ur ratio of PUs at varying strain rates.

Fig. 11 and Table 5 show the rate-dependence of the ultimate tensile stress as the ultimate tensile stress vs. the strain rate for the stresses evaluated at different strain levels for all PUs. Due to strain softening, PU2 reached its ultimate tensile stress after the elastic limit and before undergoing strain softening for strain rates exceeding 0.01 s^{-1}. The same behavior was observed for the ultimate tensile stress of PU4 at a strain rate of 0.33 s^{-1}. For all other strains, PU2 and PU4 reached their ultimate tensile stress just before their failure. PU6 and PU8 exhibited ultimate tensile stress just before failure over the strain rates tested in this study. For all tested strain levels, the ultimate tensile stress of all PUs clearly increased due to the increase in stiffness with increasing strain rates. Although PU2 exhibited the highest modulus at all strain levels, PU2 exhibited the lowest ultimate tensile value among all PUs at a strain rate of 0.001 s^{-1} due to the low strain-hardening behavior (low tangent modulus) and the low failure strain compared with other materials. However, PU2 exhibited the highest value among the four PUs for strain rates exceeding 0.1 s^{-1} because it was stiffer than the other PUs. Increasing the strain rates from 0.001 s^{-1} and 0.33 s^{-1} increased the ultimate tensile stress by factors of 3.6, 2.1, 2.1 and 1.9 for PU2, PU4, PU6, and PU8, respectively. This relationship at low to intermediate strain rates indicated that the ultimate tensile value will be further enhanced under high strain conditions.

Ductile materials are often used as strengthening and retrofitting materials for dynamic loading applications because they can absorb the energy or shock imparted by these loads. Additionally, ductile materials will usually show signs of deformation before failure when they are overloaded. In general, the conditions at the failure of any material, such as the failure stress and failure strain, are key characteristics that define its ductility. When a polymer experiences high loads, its microstructure experiences high concentrations of local stress, and the microstructurally weak regions (microstructural defects) begin to deform and form micro-scale ridges and voids within the microstructure. Due to molecular chain disentanglement, the coalescence of these ridges creates a linear distortion region with discrete voids. Consequently, these discrete voids grow, and webs are formed between the voids. As the above process propagates, the voids continue to grow, and the connections between voids create enlarged voids. When the sizes of enlarged void become critical, a crack is formed, which induces the failure of the polymer [6].

In all cases, a single break point was observed. As expected from the viscoelastic behavior of these materials, the failure stress increased and the failure strain decreased as the strain rate increased. A comparison of the failure stress to the strain rate [Fig. 12(a) and Table 6] shows trends in the failure stress attained for a given strain rate similar to those obtained in the ultimate tensile stress. In a comparison of the failure stress among the four PUs, PU4 showed the highest value for all tested strain levels due to its moderate stiffness and strain hardening characteristics in contrast to the high stiffness of PU2 and better strain hardening of PU6 and PU8. For strains rates higher than 0.05 s^{-1}, increases in the failure stress were slightly larger than those observed for strain rates ranging from 0.001 s^{-1} to 0.01 s^{-1}. As indicated earlier, this difference might have been due to reduced molecular alignment induced by stiffening at higher strain levels. The failure strains at different strain levels are plotted in Fig. 12(b) and listed in Table 7. Because these materials stiffened as the strain rates increased, a dramatic reduction in the failure strain was observed. This behavior was typical of viscoelastic materials, which tend to fail at higher stresses but lower strains when the strain rate is increased. The same trend was observed by Roland et al. [41], who investigated the uniaxial tensile behavior of elastomeric polyurea. For all strain rate levels, the failure strain directly correlated with the plasticizer content and increased from PU2 to PU8. Specifically, the addition of plasticizer lengthened the SS segments in the polymer chain, which increases the mobility of the molecular structure of the material and consequently reduces its stiffness.

Table 2
Summary of Young's module values and variations.

Strain rate (s^{-1})	Young's modules (MPa)							
	PU2		PU4		PU6		PU8	
	Avg.	Stdv.	Avg.	Stdv.	Avg.	Stdv.	Avg.	Stdv.
0.001	35.8	2.5	29.0	1.9	22.6	1.6	7.3	1.2
0.005	52.0	1.5	36.3	4.2	30.8	3.0	11.7	2.1
0.01	66.2	2.3	44.1	1.7	35.1	1.9	25.6	0.8
0.05	85.8	3.6	64.0	1.4	55.7	2.1	40.0	5.9
0.1	102.5	3.2	85.8	3.6	71.8	4.9	56.4	4.2
0.33	130.7	1.8	117.2	8.0	93.4	4.8	74.5	4.1

Table 3
Summary of yield stress values and variations.

Strain rate (s^{-1})	Yield stress (MPa)							
	PU2		PU4		PU6		PU8	
	Avg.	Stdv.	Avg.	Stdv.	Avg.	Stdv.	Avg.	Stdv.
0.001	3.8	0.1	3.5	0.2	2.9	0.2	0.9	0.2
0.005	5.4	0.3	4.6	0.1	4.0	0.1	1.4	0.2
0.01	6.8	0.2	5.2	0.3	4.6	0.2	3.0	0.3
0.05	8.6	0.4	7.8	0.3	7.4	0.3	4.4	0.2
0.1	10.1	0.2	9.7	0.8	8.7	0.5	6.2	0.2
0.33	13.6	0.2	12.8	0.7	11.0	1.0	7.2	0.2

Table 4
Summary of tangent module values and variations.

Strain rate (s^{-1})	Tangent modulus (MPa)							
	PU2		PU4		PU6		PU8	
	Avg.	Stdv.	Avg.	Stdv.	Avg.	Stdv.	Avg.	Stdv.
0.001	0.68	0.07	1.53	0.07	1.69	0.11	2.32	0.04
0.005	0.63	0.14	2.18	0.14	1.55	0.09	2.27	0.06
0.01	−1.15	0.42	2.07	0.18	1.49	0.15	2.08	0.23
0.05	−3.25	0.29	1.51	0.06	1.55	0.17	1.94	0.04
0.1	−3.43	0.38	0.89	0.87	1.47	0.75	1.85	0.17
0.33	−6.94	0.27	−1.33	0.56	0.63	0.55	1.74	0.15

Table 5
Summary of ultimate tensile stress values and variations.

Strain rate (s^{-1})	Ultimate Tensile Stress (MPa)							
	PU2		PU4		PU6		PU8	
	Avg.	Stdv.	Avg.	Stdv.	Avg.	Stdv.	Avg.	Stdv.
0.001	4.6	0.2	6.4	0.1	6.7	0.4	5.9	0.3
0.005	6.3	0.2	7.8	0.1	7.2	0.3	6.2	0.3
0.01	7.7	0.3	8.4	0.3	7.7	0.3	7.3	0.5
0.05	10.0	0.2	10.1	0.2	9.8	0.7	8.2	0.3
0.1	11.9	0.5	11.9	0.4	11.3	0.7	10.0	0.4
0.33	16.3	0.5	15.8	0.3	13.9	0.1	11.2	0.4

Table 6
Summary of failure stress values and variations.

Strain rate (s^{-1})	Failure stress (MPa)							
	PU2		PU4		PU6		PU8	
	Avg.	Stdv.	Avg.	Stdv.	Avg.	Stdv.	Avg.	Stdv.
0.001	4.6	0.2	5.7	0.1	6.0	0.4	5.0	0.4
0.005	6.0	0.2	7.2	0.2	6.6	0.3	5.3	0.2
0.01	6.4	0.4	7.8	0.3	7.3	0.3	6.4	0.7
0.05	6.8	0.5	9.4	0.3	9.1	0.7	7.6	0.3
0.1	9.5	0.3	11.2	0.4	11.0	0.7	9.4	0.3
0.33	12.9	0.5	14.5	0.2	13.3	0.1	10.9	0.3

Table 7
Summary of failure strain values and it variations.

Strain rate (s^{-1})	Failure strain							
	PU2		PU4		PU6		PU8	
	Avg.	Stdv.	Avg.	Stdv.	Avg.	Stdv.	Avg.	Stdv.
0.001	1.49	0.03	1.57	0.07	2.19	0.01	2.28	0.06
0.005	1.32	0.03	1.44	0.06	2.02	0.07	2.09	0.02
0.01	1.16	0.06	1.36	0.08	1.86	0.05	1.94	0.04
0.05	1.01	0.09	1.10	0.07	1.50	0.05	1.59	0.02
0.1	0.83	0.04	1.00	0.07	1.27	0.01	1.36	0.03
0.33	0.62	0.03	0.84	0.05	1.04	0.04	1.22	0.11

3.2. Strain energy

The ability of a material to absorb and dissipate energy are key characteristics to be considered when selecting a material for strengthening or retrofitting applications that are subjected to dynamic loads. When a force acts on a material as it deforms, the applied load is stored as strain energy throughout its volume, which results in elastic and plastic deformations within the material. In practice, numerous methods have been used to quantify the energy absorption and dissipation capacities of materials. However, the strain energy is frequently used as a measure of these capabilities of an elastomeric material, and it is defined as the internally stored energy within a material due to a change in its original shape [65]. The strain energy density is defined as the strain energy per unit volume and calculated by computing the area beneath the stress-strain curve. The cumulative strain energy densities vs. the engineering strains for varying strain rate levels are shown in Fig. 13. The strain energy density of PUs strongly depended on the rate, i.e., they absorbed higher energy at lower strains in the higher strain rate regime. Over the tested strain rate regimes, the cumulative strain energy density linearly increased with the strain after their yield point for PU2, PU4 and PU6. Although the cumulative strain energy density of PU8 linearly increased at higher strain levels, this increase deviated from linearity at lower strains due to its strain hardening behavior.

In the initial linear region (up to the proportionality limit) of the stress-strain plots, the resulting distortion caused by the applied loads was not accompanied by energy dissipation. The resilience modulus (Ur) is defined as the strain energy density in response to the elastic deformation of the material [65]. Explicitly, it can be defined as the maximum energy that can be absorbed per unit volume of the material without undergoing permanent deformation or damage. Specifically, the energy absorbed up to the proportionality limit dissipates throughout the unloading of the applied

Table 8
Summary of resilience module values and variations.

Strain rate (s^{-1})	Resilience modules							
	PU2		PU4		PU6		PU8	
	Avg.	Stdv.	Avg.	Stdv.	Avg.	Stdv.	Avg.	Stdv.
0.001	0.23	0.01	0.25	0.02	0.22	0.03	0.07	0.02
0.005	0.30	0.03	0.37	0.05	0.32	0.02	0.10	0.02
0.01	0.38	0.02	0.39	0.05	0.34	0.02	0.22	0.04
0.05	0.47	0.03	0.60	0.05	0.63	0.09	0.30	0.02
0.1	0.54	0.02	0.70	0.12	0.69	0.16	0.45	0.01
0.33	0.62	0.01	1.07	0.10	0.75	0.13	0.41	0.02

Table 9
Summary of toughness module values and variations.

Strain rate (s^{-1})	Toughness modules							
	PU2		PU4		PU6		PU8	
	Avg.	Stdv.	Avg.	Stdv.	Avg.	Stdv.	Avg.	Stdv.
0.001	6.08	0.22	8.03	0.33	9.99	0.85	7.19	0.58
0.005	7.60	0.13	8.88	0.28	11.07	0.43	7.83	0.41
0.01	7.66	0.25	9.24	0.63	11.69	1.08	9.87	0.42
0.05	8.09	0.75	9.60	0.69	12.52	0.28	9.61	0.38
0.1	8.34	0.62	10.64	0.72	12.68	0.56	11.25	0.40
0.33	8.44	0.58	11.99	0.73	13.12	0.55	11.81	1.35

Table 10
Summary of Ut/Ur ratio values and variations.

Strain rate (s^{-1})	Ut/Ur							
	PU2		PU4		PU6		PU8	
	Avg.	Stdv.	Avg.	Stdv.	Avg.	Stdv.	Avg.	Stdv.
0.001	27.0	2.3	31.8	4.1	44.5	8.1	101.4	18.4
0.005	25.5	2.3	23.8	2.7	34.4	3.1	59.2	15.5
0.01	20.2	0.8	23.7	3.3	33.9	3.9	44.9	10.1
0.05	17.0	1.8	16.1	1.5	20.0	3.3	32.3	3.0
0.1	15.4	0.9	15.3	3.4	18.4	3.2	24.8	1.4
0.33	13.6	0.8	11.2	1.6	17.4	2.7	29.0	3.7

loads. The Ur was calculated by integrating the area underneath the stress-strain plot from zero to its proportionality limit. Fig. 14 and Table 8 compare the Ur of PUs under low to intermediate strain rate regimes. Fig. 14 and Table 8 show that increasing the strain rate significantly affected the Ur, producing a dramatic increase in the logarithm of the strain rate. Generally, PU4 exhibited the highest Ur value of all the PUs.

The toughness modulus (Ut) of a material signifies its ability to absorb energy via its elastic and plastic deformation without cracking or fracturing. In another way, the Ut is defined as the strain energy density of a material immediately before failure and is computed by integrating the area underneath the stress–strain curve until failure [65]. Fig. 15 and Table 9 compare the Ut over the tested strain rates for low to intermediate strains. Over the tested regimes, the Ut gradually increased as a function of the logarithm of the strain rate for increasing strain rates. As illustrated by the graphs, PU6 showed the highest Ut value for all strain rate levels.

The data show that Ut values of the PUs were significantly higher than that of the counterpart in the elastic region. Fig. 16 and Table 10 show the ratios of the Ut to the Ur of the PUs evaluated in this study, which ranged from 10 to 100. This outcome confirms that PUs can absorb a substantial amount of energy, even if they experience plastic deformation. This characteristic is imperative for strengthening or retrofitting materials that will be used for applications under dynamic loads. Furthermore, these findings are consistent with the objectives of the current study, that is, to develop a material for strengthening of structures subject to blast and impact loading conditions. These materials absorb a considerable amount of energy and would not fail abruptly after yielding, unlike most brittle construction materials, such as masonry, concrete and ceramics. Although the Ur and Ut directly correlated with the strain rate, the Ut/Ur ratio decreased for all PUs due to the decrease in their failure strain. According to the data, PU8 showed the highest ratio for all strain levels due to its higher failure strain and low stiffness compared to the other materials. Although the differences in their ratios are large at low strain levels, the ratios are much closer in value at higher strain levels. Taken together, all the tensile characteristics indicate that the PUs can be defined as hyper-viscoelastic material.

3.3. Unloading behavior

Majority of dynamic loadings are multi-cyclic, materials undergo both loading and unloading conditions consequently. Therefore both loading and unloading behavior of these materials are highly important. Here, the loading and unloading stress–strain behaviors of four types of PUs were observed for varying strain rates. Specifically, loads up to 0.3 strain were applied, and unloading was accomplished at the same strain rate. The unloading engineering stress–strain behavior of all four PUs is highly non-linear compared with the loading, as shown in Fig. 17. Over the tested strain rate regimes, the unloading stress–strain behavior of each PU sample exhibited hysteresis during loading. The stiffness of PUs strongly depended on strain and dramatically increased for low to intermediate range strain rates, and the materials transitioned from rubbery to leathery behavior as the strain rate increased, similar to the phenomenon observed during loading. All PUs exhibited residual strain after an applied strain of 0.3 for all tested strain levels. The residual strains of PUs at different strain levels are shown in Fig. 18 and Table 11 for comparison. Over the tested strain rate regimes, the residual strain of all PUs displayed rate sensitivity, as evidenced by the small but dramatic increase as the strain rate increased. This phenomenon arose because PUs do not have sufficient time to re-align their polymer chains when the strain rate increases. Additionally, PU2, which contained lowest levels of SS, exhibited the highest residual strains, and this

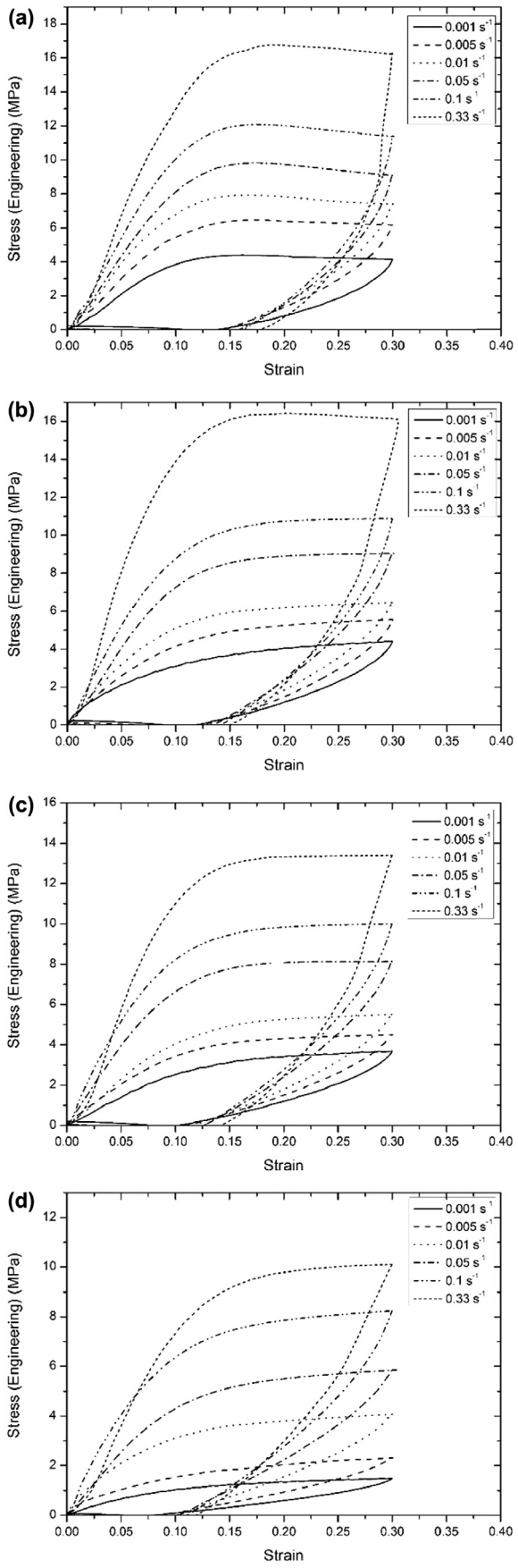

Fig. 17. The loading and unloading engineering stress-strain curves of PUs at varying strain rates; (a) PU2, (b) PU4, (c) PU6, (d) PU8.

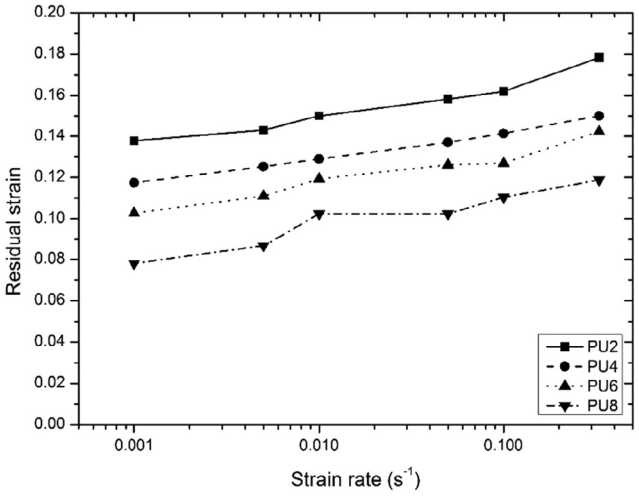

Fig. 18. The residual strain of PUs at varying strain rates.

Table 11
Summary of residual values and it variations.

Strain rate (s^{-1})	Residual Strain							
	PU2		PU4		PU6		PU8	
	Avg.	Stdv.	Avg.	Stdv.	Avg.	Stdv.	Avg.	Stdv.
0.001	0.138	0.011	0.118	0.006	0.103	0.009	0.078	0.005
0.005	0.143	0.009	0.125	0.008	0.111	0.007	0.087	0.005
0.01	0.150	0.010	0.129	0.006	0.119	0.009	0.102	0.008
0.05	0.158	0.012	0.137	0.011	0.126	0.005	0.102	0.006
0.1	0.162	0.007	0.141	0.013	0.127	0.007	0.110	0.007
0.33	0.178	0.007	0.150	0.010	0.142	0.009	0.119	0.005

residual strain inversely correlated with the content of SS, decreasing from PU2 to PU8.

3.4. Cyclic softening

Elastomeric materials exhibit cyclic softening behavior due to the breakdown and reorganization of segregated hard segments in response to strain. Because PU6 was shown the best co-relation for a strengthening material for dynamic applications, the cyclic softening behavior of only PU6 was examined to limit the scope of the study. In order to understand the effect of the strain rate on the softening behavior, each PU6 specimen was subjected to 5 consecutive loading–unloading-reloading cycles with a maximum strain of 0.3 for three strain rates, 0.001, 0.01 and 0.1 s^{-1}. No dwell time was allowed as the strain direction was changed. Fig. 19 plots the uniaxial tensile stress-strain behavior during cyclic tests for the strain rates mentioned above. The obtained data were used to obtain the stress softening behavior, which was computed from the stress at the maximum strain (0.3) for each cycle and is expressed as the relative stress softening (σ_n*), i.e., the ratio of the stresses at the maximum strain (0.3) of n^{th} cycle (σ_1) to the stress at the maximum strain (0.3) of the first cycle (σ_n). Different measures of the specific work input (W) were computed by integrating the stress-strain curve up to the maximum strain. The difference between the loading and unloading strain–stress path shows the dissipated energy or the hysteresis loss and was computed by integrating both loading and unloading stress-strain curves [27]. The first cycle work input (W_1) was computed by integrating the first loading up to 0.3 strain, and the first cycle hysteresis (ΔW_1) was calculated by integrating the first loading and unloading curve up to its residual strain. Subsequent cycle

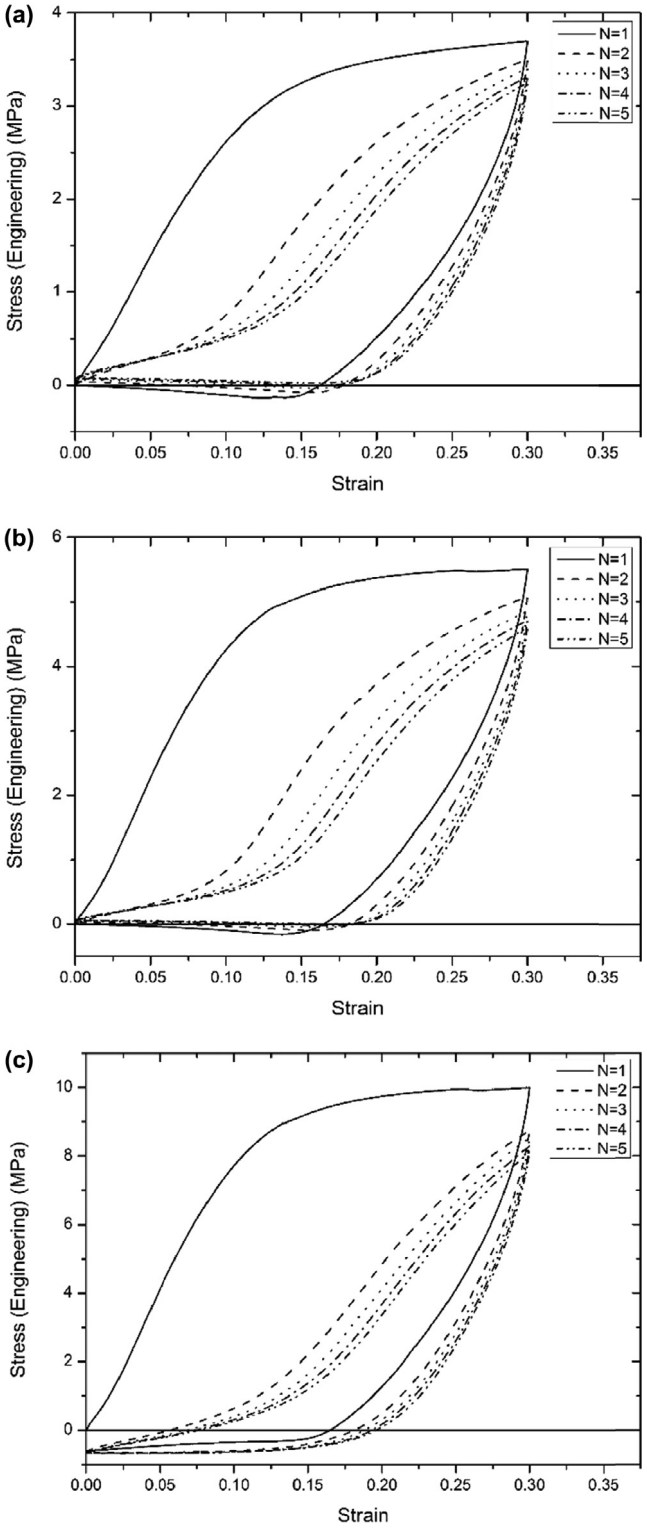

Fig. 19. The cyclic softening engineering stress-strain curves of PU6 at varying strain rates; (a) 0.001 s^{-1}, (b) 0.01 s^{-1}, (c) 0.1 s^{-1}.

work inputs (W_n; n = 2, 3, 4, and 5) were obtained by integrating each stress–strain curve up to 0.3 and subsequent cycle hystereses (ΔW_n; n = 2, 3, 4, and 5) were computed by integrating the respective loading-unloading curve. When comparing the behavior under different strain conditions, the work outputs and cycle hysteresis were expressed in various ways, such as the relative hysteresis, ΔW_n^* (hysteresis/work input), relative work input compared to

Table 12
Tensile test results of PU6 for different loading/unloading cycles to nominal strain of 0.3., and nominal strain rate 0.001 s^{-1}.

Cycle no (n)	σ_n(Nm^{-2})	σ_{n*}	W_n (MJm^{-3})	ΔW_n (MJm^{-3})	ΔW_n^*	$W_{n/1}^*$	$\Delta W_{n/1}^*$
1	3.70	–	0.81	0.64	0.78	–	–
2	3.50	0.95	0.52	0.38	0.73	0.63	0.59
3	3.40	0.92	0.45	0.32	0.71	0.53	0.50
4	3.32	0.90	0.42	0.30	0.70	0.52	0.46
5	3.25	0.88	0.40	0.28	0.70	0.49	0.44

Table 13
Tensile test results of PU6 for different loading/unloading cycles to nominal strain of 0.3., and nominal strain rate 0.01 s^{-1}.

Cycle no (n)	σ_n(Nm^{-2})	σ_{n*}	W_n (MJm^{-3})	ΔW_n (MJm^{-3})	ΔW_n^*	$W_{n/1}^*$	$\Delta W_{n/1}^*$
1	5.51	–	1.27	1.01	0.80	–	–
2	5.08	0.92	0.72	0.51	0.71	0.57	0.51
3	4.85	0.88	0.61	0.43	0.70	0.48	0.43
4	4.72	0.86	0.56	0.39	0.70	0.44	0.39
5	4.60	0.83	0.52	0.36	0.69	0.41	0.36

Table 14
Tensile test results of PU6 for different loading/unloading cycles to nominal strain of 0.3., and nominal strain rate 0.1 s^{-1}.

Cycle no (n)	σ_n (Nm^{-2})	σ_{n*}	W_n (MJm^{-3})	ΔW_n (MJm^{-3})	ΔW_n^*	$W_{n/1}^*$	$\Delta W_{n/1}^*$
1	9.99	–	2.30	1.83	0.80	–	–
2	8.75	0.88	0.95	0.60	0.62	0.42	0.33
3	8.53	0.85	0.85	0.52	0.61	0.37	0.28
4	8.29	0.83	0.78	0.48	0.61	0.34	0.26
5	8.11	8.31	0.74	0.45	0.60	0.32	0.24

the first cycle work input $W_{n/1}^*$ (work input/ first cycle work input), relative hysteresis compared to the first cycle work input $\Delta W_{n/1}^*$ (hysteresis/first cycle hysteresis). The computed values for strains of 0.001, 0.01, and 0.1 s^{-1} are tabulated in Table 12, 13 and 14, respectively.

More compliant behavior was observed in the reloading stress–strain curves compared to the initial loading behavior due to the partial breakdown and transformation of hard segments into soft segment, which results in material softening. PU6 exhibited the Mullins effect, for which the first loading is associated with higher stiffness and hysteresis. The initial loading changes the microstructure when the strain exceeds the elastic limit, such that following loads inside the previous deformation envelope are associated with lower stiffness and hysteresis than the initial load because the microstructure of PU changes during each subsequent cycle. As stated above, this new microstructure formed due to the stripping and fragmentation of HS in the hard phase, which then combines with the soft phase [19]. Accordingly, the stress-strain path of re-loading more closely follows the previous unloading path compared with the first loading path. In addition, although PU6 significantly softened during the first few cycles, the cycles did not exhibit noticeable differences in the unloading paths. Hence, the unloading stress-strain behavior of PU6 does not significantly depend on the deformation history. Moreover, Tables 12–14 clearly show that the relative stress softening directly correlated with the strain rate and that the relative hysteresis loss converges to a specific value for all strain levels tested. The stress-strain curves tend to stabilize on a fixed trajectory after a few loading and unloading cycles, and the same behavior was observed by Qi and Boyce [35] in their studies. Additionally, Bartolomé et al. [27] reported that the stress softening mechanism and its stability depend on the maximum strain reached and the HS and SS contents. The relative hysteresis loss depended on the deformation state tested (Tables 12–14); particularly, the relative hysteresis loss directly correlated with the strain rate over the studied range.

Fig. 19 shows the direct relationship between the residual strain and the cycle number and the stability of the residual strain after first cycle for each strain rate. Consequently, the residual strain rapidly converged at lower strain rates. Conversely, the literature reports relative stress softening, and the relative residual strains also depend on the maximum strain reached and generally increase with the maximum strain [27]. At the 0.1 s^{-1} strain level, initial compression stress was observed after first cycle of loading. This phenomenon may be due to the insufficient time to release the residual strain caused compression stress until the material reaches the original length plus the residual strain during reloading. To study the degree of strain recovery of PU6, the gauge lengths of deformed specimens were re-measured 1 day after testing to measure the permanent strain. The residual strains recovered due to long-term effects, and the same observations were obtained by Blundell et al. [63] and Qi and Boyce [35] for several PUs. Large strain recovery under a wide range of loading, including quasi-static to impact (under varying strain rates) make the PU feasible for coating on concrete to enhance the flexural capacity and resistance against under varying loads including dynamic loadings.

4. Conclusions

This work investigated the uniaxial tensile behavior of four types of PUs with varying soft segment ratios under low to intermediate strain rate regimes (0.001–0.33 s^{-1}). This nonlinear and rate dependent behavior was investigated by focusing on material parameters such as tensile characteristics, strain energy, unloading behavior, and cyclic softening. A dramatic transition in behavior from rubbery to leathery was observed in response to increasing strain rates for all PUs. Young's modulus, the yield stress, the maximum tensile stress, the failure stress, and the resilience and toughness moduli directly correlated with the strain rate, whereas the tangent modulus and failure strain inversely correlated with the strain rate. Among the four tested PUs, PU2 (with 2% of plasticizer with respect to the weight of

polyol) exhibited high stiffness but low toughness, and PU8 (with 8% of plasticizer with respect to the weight of polyol) exhibited high toughness but low stiffness. The observed increase in the strain energy density as the strain rate increased suggests that these materials absorb more energy under dynamic loads. PU6 exhibited desirable stiffness and toughness qualities together with the best energy absorption characteristics over the tested regimes based on the Ut value, making it acceptable as a strengthening or retrofitting material for dynamic applications, including blast and ballistic applications. The stoichiometry strongly influenced the mechanical response of PU due to the complex interplay of crosslinking, the content of soft and hard segments, the degree of phase separation, and hydrogen-bond formation. In this study, slight changes in the chemistry of PU due to changes in the SS content (plasticizer content changed by 2–8%) produced large changes in the mechanical response. Specifically, Young's modulus and yield stress inversely correlated with the content of SS, whereas the failure strain directly correlated with the content of SS. These results highlighted the necessity of controlling the stoichiometry of PU to attain desirable properties suitable for dynamic applications. The behavior of PUs can be defined as hyper-viscoelastic material.

The unloading engineering stress–strain behavior of all four PUs was highly non-linear compared with the loading behavior. Over the tested strain rate regimes, the residual strain of all PUs exhibited rate sensitivity, as evidenced by the small dramatic increase in response to an increasing strain rate. PU8, which featured the lowest soft segment content, exhibited the highest residual strains, and the residual strain decreased as the SS content increased from PU2 to PU8. Among the four PUs tested, PU 6 (with 6% of plasticizer with respect to the weight of polyol) showed the best performance under overall tensile characteristics.

PU6 exhibited the Mullins effect, showing softening during the first cycles of loading that became insignificant in subsequent cycles. In addition, although PU6 significantly softened during the first few cycles, differences in the unloading paths were not observed between cycles. Hence, the unloading stress-strain behavior of PUs was not significantly dependent on the deformation history. The softening was more significant for higher strain levels than for lower strain levels. Moreover, the stress-strain curves tended to stabilize on a fixed trajectory after a few cycles of loading and unloading, and the residual strain also stabilized after the first cycle for each strain level.

The findings of this study suggest that bio-based PU elastomer may be applied effectively as a protective coating material for strengthening concrete structures under blast and impact loadings. This will enhance flexural capacity of concrete structures, which results in higher resistance against aforementioned impact loads and control damage sustained by the reduction of the crushing and fragmentation of reinforced concrete structures. PU6 has the highest potential to be used as strengthening material in concrete considering its overall behavior, dynamic tensile properties, energy absorption and dissipation abilities, unloading and strain recovery abilities, and cyclic softening behavior.

Acknowledgement

The authors would like to extend their gratitude to Universiti Kebangsaan Malaysia and the Ministry of Higher Education, Malaysia for providing the necessary funding for this research through Impak Perdana Grant (DIP-2017-002), and to the Polymer Research Centre of UKM for the generous supply of palm-based polyol.

References

[1] D.K.K. Chattopadhyay, K.V.S.N. Raju, Structural engineering of polyurethane coatings for high performance applications, Prog. Polym. Sci. 32 (2007) 352–418, https://doi.org/10.1016/j.progpolymsci.2006.05.003.
[2] H.M.C.C. Somarathna, S.N. Raman, D. Mohotti, A.A. Mutalib, K.H. Badri, The use of polyurethane for structural and infrastructural engineering applications: a state-of-the-art review, Constr. Build. Mater. 190 (2018) 995–1014, https://doi.org/10.1016/j.conbuildmat.2018.09.166.
[3] H.M.C.C. Somarathna, S.N. Raman, A.A. Mutalib, K.H. Badri, Elastomeric polymers for blast and ballistic retrofitting of structures, J. Teknol. 76 (2015), https://doi.org/10.11113/jt.v76.3608.
[4] A.F. Saleeb, S.H. Natsheh, J.S. Owusu-Danquah, A multi-mechanism model for large-strain thermomechanical behavior of polyurethane shape memory polymer, Polymer (Guildf). 130 (2017) 230–241, https://doi.org/10.1016/j.polymer.2017.10.003.
[5] M. Grujicic, B. Pandurangan, T. He, B.a. Cheeseman, C.-F. Yen, C.L. Randow, Computational investigation of impact energy absorption capability of polyurea coatings via deformation-induced glass transition, Mater. Sci. Eng. A. 527 (2010) 7741–7751, https://doi.org/10.1016/j.msea.2010.08.042.
[6] J.T. Fan, J. Weerheijm, L.J. Sluys, High-strain-rate tensile mechanical response of a polyurethane elastomeric material, Polym. (United Kingdom) 65 (2015) 72–80, https://doi.org/10.1016/j.polymer.2015.03.046.
[7] J.T. Fan, J. Weerheijm, L.J. Sluys, Glass interface effect on high-strain-rate tensile response of a soft polyurethane elastomeric polymer material, Compos. Sci. Technol. 118 (2015) 55–62, https://doi.org/10.1016/j.compscitech.2015.08.007.
[8] J. Choi, D.S. Moon, J.U. Jang, W. Bin Yin, B. Lee, K.J. Lee, Synthesis of highly functionalized thermoplastic polyurethanes and their potential applications, Polymer (Guildf) 116 (2017) 287–294, https://doi.org/10.1016/j.polymer.2017.03.083.
[9] J.S. Davidson, J.R. Porter, R.J. Dinan, M.I. Hammons, J.D. Connell, Explosive testing of polymer retrofit masonry walls, J. Perform. Constr. Facil 18 (2004) 100–106, https://doi.org/10.1061/(ASCE)0887-3828(2004)18:2(100).
[10] T.D. Hrynyk, J.J. Myers, F. Asce, Out-of-Plane Behavior of URM Arching Walls with Modern Blast Retrofits: Experimental Results and Analytical Model, (2008) 1589–1597
[11] D. Mohotti, T. Ngo, S.N. Raman, M. Ali, P. Mendis, Plastic deformation of polyurea coated composite aluminium plates subjected to low velocity impact, Mater. Des. 56 (2014) 696–713, https://doi.org/10.1016/j.matdes.2013.11.063.
[12] D. Mohotti, M. Ali, T. Ngo, J. Lu, P. Mendis, D. Ruan, Out-of-plane impact resistance of aluminium plates subjected to low velocity impacts, Mater. Des. 50 (2013) 413–426, https://doi.org/10.1016/j.matdes.2013.03.023.
[13] M.R. Amini, J.B. Isaacs, S. Nemat-Nasser, Experimental investigation of response of monolithic and bilayer plates to impulsive loads, Int. J. Impact Eng. 37 (2010) 82–89, https://doi.org/10.1016/j.ijimpeng.2009.04.002.
[14] M.R. Amini, J. Isaacs, S. Nemat-Nasser, Investigation of effect of polyurea on response of steel plates to impulsive loads in direct pressure-pulse experiments, Mech. Mater. 42 (2010) 628–639, https://doi.org/10.1016/j.mechmat.2009.09.008.
[15] K. Ackland, C. Anderson, T.D. Ngo, T. Duc, Deformation of polyurea-coated steel plates under localised blast loading, Int. J. Impact Eng. 51 (2013) 13–22, https://doi.org/10.1016/J.IJIMPENG.2012.08.005.
[16] M. Grujicic, B. Pandurangan, B. d'Entremont, The role of adhesive in the ballistic/structural performance of ceramic/polymer–matrix composite hybrid armor, Mater. Des. 41 (2012) 380–393, https://doi.org/10.1016/j.matdes.2012.05.023.
[17] Y.A. Bahei-El-Din, G.J. Dvorak, Behavior of sandwich plates reinforced with polyurethane/polyurea interlayers under blast loads, J. Sandw. Struct. Mater. 9 (2007) 261–281, https://doi.org/10.1177/1099636207066313.
[18] S.N. Raman, Polymeric Coatings for Enhanced Protection of Reinforced Concrete Structures from the Effects of Blast PhD Thesis, Department of Civil and Environmental Engineering, The University of Melbourne, Australia, 2011.
[19] S.N. Raman, H.M.C.C. Somarathna, A.A. Mutalib, K.H. Badri, M.R. Taha, Bio-based polyurethane elastomer for strengthening application of concrete structures under dynamic loadings, in: Int. Congr. Polym. Concr. (ICPIC 2018), Springer International Publishing, Cham, 2018, pp. 751–757, https://doi.org/10.1007/978-3-319-78175-4_96.
[20] H.M.C.C. Somarathna, S.N. Raman, D. Mohotti, A.A. Mutalib, K.H. Badri, Hyper-viscoelastic constitutive models for predicting the material behavior of polyurethane under varying strain rates and uniaxial tensile loading, Constr. Build. Mater. 236 (2020), https://doi.org/10.1016/j.conbuildmat.2019.117417 117417.
[21] S.N. Raman, T. Pham, T. Ngo, P. Mendis. (2012). Experimental Investigation on the Behaviour of RC Panels Retrofitted with Polymer Coatings under Blast Effects. Proceedings of the 2nd International Conference on Sustainable Built Environment: 14 pgs. Kandy, Sri Lanka, 14–16 December 2012.
[22] S. N. Raman, H. M. C. C. Somarathna, A. A. Mutalib, K. H. Badri. (2017). "Elastomeric Polyurethane for Retrofitting Application of Concrete Structures under Dynamic Loading". RILEM Proceedings 118: Advances in Construction Materials and Systems – Vol. 2 (ICACMS2017): pp. 549–556. Chennai, India, 3–8 September 2017.
[23] Z.S. Pztrovic, J. Ferguson, Polyurethane elastomers, Prog. Polym. Sci. 16 (1991) 695–836, https://doi.org/10.1016/0079-6700(91)90011-9.

[24] C.P. Buckley, C. Prisacariu, C. Martin, Elasticity and inelasticity of thermoplastic polyurethane elastomers: Sensitivity to chemical and physical structure, Polymer (Guildf). 51 (2010) 3213–3224, https://doi.org/10.1016/j.polymer.2010.04.069.
[25] R. Bonart, Thermoplastic Elastomers, Encycl. Polym. Sci. Technol. 20 (1979) 1389–1403, https://doi.org/10.1002/0471440264.pst105.
[26] H.F.F. Enderle, H.G.G. Kilian, B. Heise, J. Mayer, H. Hespe, Irreversible deformation of semicrystalline PUR-elastomers -a novel concept, Colloid Polym. Sci. 264 (1986) 305–322, https://doi.org/10.1007/BF01418190.
[27] L. Bartolomé, J. Aurrekoetxea, M.A. Urchegui, W. Tato, The influences of deformation state and experimental conditions on inelastic behaviour of an extruded thermoplastic polyurethane elastomer, Mater. Des. 49 (2013) 974–980, https://doi.org/10.1016/j.matdes.2013.02.055.
[28] F. Yeh, B.S. Hsiao, B.B. Sauer, S. Michel, H.W. Siesler, In-Situ Studies of Structure Development during Deformation of a Segmented Poly (urethane – urea) Elastomer (2003) 1940–1954.
[29] H.M.C.C. Somarathna, S.N. Raman, K.H. Badri, A.A. Mutalib, D. Mohotti, S. Engineering, S.D. Ravana, Quasi-static behavior of palm-based elastomeric polyurethane: for strengthening application of Structures under impulsive loadings, Polymers (Basel). (2016), https://doi.org/10.3390/polym8050202.
[30] J. Furmanski, C.P. Trujillo, D.T. Martinez, G.T.G. Iii, E.N. Brown, Dynamic-Tensile-Extrusion for investigating large strain and high strain rate behavior of polymers, Polym. Test. 31 (2012) 1031–1037, https://doi.org/10.1016/j.polymertesting.2012.07.011.
[31] M. Lonesuc, Chemistry and Technology of Polyols for Polyurethanes, Rapa Technology Limited, Shawbury, Shrewabury, Shropshire, SY4 4NR, UK, 2005.
[32] H.M.C.C. Somarathna, S.N. Raman, A.A. Mutalib, K.H. Badri, Mechanical characterization of polyurethane elastomers: for retrofitting application against blast effects, in: Proceedins Third Conf. Smart Monit. Assess. Rehabil. Struct. (SMAR 2015), Antalya, Turkey, 2015, pp. 82–89.
[33] C. Prisacariu, R.H. Olley, A.A. Caraculacu, D.C. Bassett, C. Martin, The effect of hard segment ordering in copolyurethane elastomers obtained by using simultaneously two types of diisocyanates, Polymer (Guildf). 44 (2003) 5407–5421, https://doi.org/10.1016/S0032-3861(03)00489-0.
[34] C. Prisacariu, C.P. Buckley, A.A. Caraculacu, Mechanical response of dibenzyl-based polyurethanes with diol chain extension, Polymer (Guildf). 46 (2005) 3884–3894, https://doi.org/10.1016/j.polymer.2005.03.046.
[35] H.J. Qi, M.C. Boyce, Stress-Strain Behavior of Thermoplastic Polyurethane Stress-Strain Behavior of Thermoplastic (2004) 1–51
[36] M. Furukawa, Y. Mitsui, T. Fukumaru, K. Kojio, Microphase-separated structure and mechanical properties of novel polyurethane elastomers prepared with ether based diisocyanate, Polymer (Guildf). 46 (2005) 10817–10822, https://doi.org/10.1016/j.polymer.2005.09.009.
[37] K. Kojio, M. Furukawa, Y. Nonaka, S. Nakamura, Control of mechanical properties of thermoplastic polyurethane elastomers by restriction of crystallization of soft segment, Materials (Basel). 3 (2010) 5097–5110, https://doi.org/10.3390/ma3125097.
[38] M.F. Sonnenschein, V.V. Ginzburg, K.S. Schiller, B.L. Wendt, Design, polymerization, and properties of high performance thermoplastic polyurethane elastomers from seed-oil derived soft segments, Polym. (United Kingdom) 54 (2013) 1350–1360, https://doi.org/10.1016/j.polymer.2012.12.077.
[39] Z. Jia, G. Yuan, D. Hui, X. Feng, Y. Zou, Effect of high strain rate and low temperature on mode II fracture toughness of ductile adhesive, Int. J. Adhes. Adhes. 86 (2018) 105–112, https://doi.org/10.1016/J.IJADHADH.2018.09.003.
[40] H. Wang, J. Yu, H. Fang, H. Wei, X. Wang, Y. Ding, Largely improved mechanical properties of a biodegradable polyurethane elastomer via polylactide stereocomplexation, Polymer (Guildf). 137 (2018) 1–12, https://doi.org/10.1016/j.polymer.2017.12.067.
[41] C.M. Roland, J.N. Twigg, Y. Vu, P.H. Mott, High strain rate mechanical behavior of polyurea, 48 (2007) 574–578. doi:10.1016/j.polymer.2006.11.051.
[42] H.M.C.C. Somarathna, S.N. Raman, A.A. Mutalib, K.H. Badri, Analysis of Strain Rate Dependent Tensile Behaviour of Polyurethanes, Proc. Int. Conf. Struct. Eng. Constr. Manag., Kandy, Sri Lanka (2015). p. 7 pgs.
[43] J.M.L. Reis, F.L. Chaves, H.S. Da Costa Mattos, Tensile behaviour of glass fibre reinforced polyurethane at different strain rates, Mater. Des. 49 (2013) 192–196, https://doi.org/10.1016/j.matdes.2013.01.065.
[44] S. Gurusideswar, R. Velmurugan, N.K. Gupta, High strain rate sensitivity of epoxy/clay nanocomposites using non-contact strain measurement, Polymer (Guildf). 86 (2016) 197–207, https://doi.org/10.1016/j.polymer.2015.12.054.
[45] J. Yi, M.C. Boyce, G.F. Lee, E. Balizer, Large deformation rate-dependent stress – strain behavior of polyurea and polyurethanes, Polymer (Guildf). 47 (2006) 319–329, https://doi.org/10.1016/j.polymer.2005.10.107.
[46] S.S. Sarva, S. Deschanel, M.C. Boyce, W. Chen, Stress e strain behavior of a polyurea and a polyurethane from low to high strain rates 48 (2007) 2208–2213. doi:10.1016/j.polymer.2007.02.058.
[47] J. Shim, D. Mohr, Using split Hopkinson pressure bars to perform large strain compression tests on polyurea at low, intermediate and high strain rates, Int. J. Impact Eng. 36 (2009) 1116–1127, https://doi.org/10.1016/j.ijimpeng.2008.12.010.
[48] M.F. Omar, H.M. Akil, Z.A. Ahmad, Measurement and prediction of compressive properties of polymers at high strain rate loading, Mater. Des. 32 (2011) 4207–4215, https://doi.org/10.1016/j.matdes.2011.04.037.
[49] N.K. Naik, P.J. Shankar, V.R. Kavala, G. Ravikumar, J.R. Pothnis, H. Arya, High strain rate mechanical behavior of epoxy under compressive loading: experimental and modeling studies, Mater. Sci. Eng., A 528 (2011) 846–854, https://doi.org/10.1016/j.msea.2010.10.099.
[50] P. Yu, X. Yao, Q. Han, S. Zang, Y. Gu, A visco-elastoplastic constitutive model for large deformation response of polycarbonate over a wide range of strain rates and temperatures, Polym. (United Kingdom) 55 (2014) 6577–6593, https://doi.org/10.1016/j.polymer.2014.09.071.
[51] L. Zhang, X. Yao, S. Zang, Q. Han, Temperature and strain rate dependent tensile behavior of a transparent polyurethane interlayer, Mater. Des. 65 (2015) 1181–1188, https://doi.org/10.1016/j.matdes.2014.08.054.
[52] G. Ravikumar, J.R. Pothnis, M. Joshi, K. Akella, S. Kumar, N.K. Naik, Analytical and experimental studies on mechanical behavior of composites under high strain rate compressive loading, Mater. Des. 44 (2013) 246–255, https://doi.org/10.1016/j.matdes.2012.07.040.
[53] Q.Z. Fang, T.J. Wang, H.G. Beom, H.P. Zhao, Rate-dependent large deformation behavior of PC/ABS, Polymer (Guildf). 50 (2009) 296–304, https://doi.org/10.1016/j.polymer.2008.10.042.
[54] S.N. Raman, T. Ngo, J. Lu, P. Mendis, Experimental investigation on the tensile behavior of polyurea at high strain rates, Mater. Des. 50 (2013) 124–129, https://doi.org/10.1016/j.matdes.2013.02.063.
[55] Z. Liao, X. Yao, Temperature and strain rate dependent large tensile deformation and tensile failure behavior of transparent polyurethane at intermediate strain rates, Int. J. Impact Eng. 129 (2019) 152–167, https://doi.org/10.1016/j.ijimpeng.2019.03.005.
[56] H. Cho, S. Bartyczak, W. Mock, M.C. Boyce, Dissipation and resilience of elastomeric segmented copolymers under extreme strain rates, Polym. (United Kingdom) 54 (2013) 5952–5964, https://doi.org/10.1016/j.polymer.2013.08.012.
[57] M.S.H. Fatt, I. Bekar, High-speed testing and material modeling of unfilled styrene butadiene vulcanizates at impact rates, J. Mater. Sci. 39 (2004) 6885–6899, https://doi.org/10.1023/B:JMSC.0000047530.86758.b9.
[58] Dong Ruan, Ming Yan Leung, Lu. Guoxing, Yu. Tongxi, Jinan Cao, a.S. Blicblau, Impact tests on lincoln wool fibers using a mini split hopkinson tensile bar, Text. Res. J. 79 (2009) 444–452, https://doi.org/10.1177/0040517508095610.
[59] J.T. Fan, J. Weerheijm, L.J. Sluys, Compressive response of multiple-particles-polymer systems at various strain rates, Polym. (United Kingdom) 91 (2016) 62–73, https://doi.org/10.1016/j.polymer.2016.03.041.
[60] Julia De Castro San Román, System Ductility and Redundancy of FRP Structures with Ductile Adhesively-Bonded Joints, Federal Institute of Technology in Lausanne, 2005.
[61] K. Haji, Biobased polyurethane from palm kernel oil-based polyol, Polyurethane (2012) 447–470, https://doi.org/10.5772/47966.
[62] C.S. Wong, Chemical analyses of palm kernel oil-based polyurethane prepolymer, Mater. Sci. Appl. 03 (2012) 78–86, https://doi.org/10.4236/msa.2012.32012.
[63] D.J. Blundell, G. Eeckhaut, W. Fuller, A. Mahendrasingam, C. Martin, Real time SAXS/stress-strain studies of thermoplastic polyurethanes at large strains, Polymer (Guildf). 43 (2002) 5197–5207, https://doi.org/10.1016/S0032-3861(02)00386-5.
[64] W.D. Callister, D.G. Rethwisch, Materials science and engineering: an introduction, n.d.
[65] R.C. Hibbeler, in: Mechanics of Materials, Pearson-Prentice Hall, Singapore, 2011, https://doi.org/10.1017/CBO9781107415324.004.